Hubbard physics with Rydberg atoms: Using a quantum spin simulator to simulate strong fermionic correlations

Antoine Michel [1,2,*] Loïc Henriet,[3] Christophe Domain [1] Antoine Browaeys,[2] and Thomas Ayral [4]

[1]*Electricité de France, EDF Recherche et Développement, Département Matériaux et Mécanique des Composants, Les Renardières, F-77250 Moret sur Loing, France*

[2]*Université Paris-Saclay, Institut d'Optique Graduate School, CNRS, Laboratoire Charles Fabry, F-91127 Palaiseau Cedex, France*

[3]*PASQAL, 7 rue Léonard de Vinci, F-91300 Massy, France*

[4]*Eviden Quantum Laboratory, 78340 Les Clayes-sous-Bois, France*

(Received 13 December 2023; revised 19 March 2024; accepted 15 April 2024; published 6 May 2024)

We propose a hybrid quantum-classical method to investigate the equilibrium physics and the dynamics of strongly correlated fermionic models with spin-based quantum processors. Our proposal avoids the usual pitfalls of fermion-to-spin mappings thanks to a slave-spin method which allows to approximate the original Hamiltonian into a sum of self-correlated free fermions and spin Hamiltonians. Taking as an example a Rydberg-based analog quantum processor to solve the interacting spin model, we avoid the challenges of variational algorithms or Trotterization methods. We explore the robustness of the method to experimental imperfections by applying it to the half-filled, single-orbital Hubbard model on the square lattice in and out of equilibrium. We show, through realistic numerical simulations of current Rydberg processors, that the method yields quantitatively viable results even in the presence of imperfections: it allows to gain insights into equilibrium Mott physics as well as the dynamics under interaction quenches. This method thus paves the way to the investigation of physical regimes, whether out of equilibrium, doped, or multiorbital, that are difficult to explore with classical processors.

DOI: 10.1103/PhysRevB.109.174409

I. INTRODUCTION

Decades of theoretical efforts have led to tremendous progress in the understanding of the exotic phases of strongly correlated electron systems. For instance, lots is known about the physics of their minimal model, the Hubbard model [1,2]. Yet, the exponential difficulty of the underlying many-body problem still poses formidable challenges in low-temperature, doped phases relevant to cuprate superconductors, in multiorbital settings relevant, for instance, to iron-based superconductors [3] and the recent Moiré superconductors [4], or in out-of-equilibrium situations like sudden quenches that lead to a fast growth of entanglement [5].

Quantum processors, i.e., controllable, synthetic quantum many-body systems [6], are promising to solve these outstanding challenges [7]. Ultracold fermionic atoms trapped in optical lattices were already implemented more than a decade ago [8–17] as the most direct, or "analog," quantum processors of fermions. They allowed to observe signatures of, for instance, Mott physics, while operating, so far, at temperatures too high to gain insights into pseudogap or superconducting phases.

In contrast, universal "digital" quantum processors rely on quantum bits encoded on two-level or "spin-$\frac{1}{2}$" systems, and operate logic gates on them. They in principle enable the simulation of the second-quantized fermionic problems explored in materials science [18] or chemistry [19]. Yet, early attempts are facing the physical limitations of these processors in terms of the number of qubits and number of gates that can be reliably executed before decoherence sets in. Fermionic systems are particularly demanding due to the loss of locality of the Hamiltonian [20,21] or the need for auxiliary qubits [22–24] that come with translating to a qubit language. Both constraints generically lead to longer quantum programs, and hence an increased sensitivity to imperfections. To alleviate those issues, hybrid quantum-classical methods [25,26] such as the variational quantum eigensolver (VQE, [27]) were proposed, with many developments but without clear-cut advantage so far.

Despite remarkable recent progress towards large-size digital quantum processors, "analog" quantum processors remain a serious alternative to explore fermionic problems. Beyond the aforementioned ultracold atoms, analog platforms include systems of trapped ions and cold Rydberg atoms. The lesser degree of control of these processors, with a fixed, specific "resource" Hamiltonian that does not necessarily match the "target" Hamiltonian of interest, is compensated for by the large number of particles that can be controlled, with now up to a few hundreds of particles [28–30]. In addition, the parameters of the resource Hamiltonian are usually precisely controlled in time [28,31–35]. This has enabled the use of such processors to study many-body problems in several recent works [34–38]. For instance, [36] have investigated the physics of the Schwinger model, a toy problem for lattice quantum electrodynamics, by leveraging the similarity between the symmetries of a 20-ion quantum simulator and those of the Schwinger model.

*antoine.michel@edf.fr

However, finding such a similarity between target and resource Hamiltonian is rare. For instance, the question of how to tackle a fermionic many-body problem with a spin-based, analog simulator is an open problem.

In this paper, we propose a method to address this problem considering a specific processor, namely, an analog Rydberg quantum processor [33,39]. By using a self-consistent mapping between the fermionic problem and a "slave-spin" model, we circumvent the nonlocality issues related to fermion-to-spin transformations. We show that the method allows one to compute key properties of the Hubbard model in and out of equilibrium. We show, through realistic numerical simulations, that it does so even in the presence of hardware imperfections like decoherence, readout error, and finite-sampling shot noise.

II. THEORY

A. The slave-spin method

As a proof of concept, we consider the single-band, half-filled Fermi-Hubbard model on a square lattice. Its Hamiltonian,

$$H_{\text{Hubbard}} = \sum_{i,j,\sigma} t_{ij} d^\dagger_{i\sigma} d_{j\sigma} + \frac{U}{2} \sum_i \left(n^d_i - 1\right)^2, \tag{1}$$

contains creation (respectively annihilation) operators $d^\dagger_{i\sigma}$ (respectively $d_{i\sigma}$) that create (respectively annihilate) an electron of spin σ on lattice site i, with a hopping amplitude t_{ij} between two sites (we will focus on nearest-neighbor hopping only, $t_{ij} = -t\delta_{\langle ij\rangle}$) and an onsite interaction U. The chemical potential was set to $\mu = U/2$ to enforce half-filling.

This prototypical model of strongly correlated electrons is hard to solve on classical processors [40], especially in out-of-equilibrium situations where the most advanced methods are usually limited to short-time dynamics. Instead of directly tackling this fermionic model, we thus resort to a separation of variables that singles out two degrees of freedom of the model, namely, spin and charge. This is achieved by resorting to a "slave-particle" method known as Z_2 slave-spin theory [41]. We replace the fermionic operator $d^\dagger_{i\sigma}$ by the product of a pseudofermion operator $f^\dagger_{i\sigma}$ and an auxiliary spin operator S^z_i ($S^{a=x,y,z}_i$ denote the Pauli spin operators), namely, $d^\dagger_{i\sigma} = S^z_i f^\dagger_{i\sigma}$. The ensuing enlargement of the Hilbert space is compensated for by imposing constraints $S^x_i + 1 = 2(n^f_i - 1)^2$ on each site. In our case, namely the single-orbital, half-filled Hubbard model on a square, i.e., bipartite, lattice, particle-hole symmetry holds, which is a sufficient condition for the constraint to be automatically satisfied [42].

We then perform a mean-field decoupling of the pseudofermion and spin degrees of freedom $S^z_i S^z_j f^\dagger_{i,\sigma} f_{j,\sigma} \approx \langle S^z_i S^z_j\rangle f^\dagger_{i,\sigma} f_{j,\sigma} + S^z_i S^z_j \langle f^\dagger_{i,\sigma} f_{j,\sigma}\rangle - \langle S^z_i S^z_j\rangle \langle f^\dagger_{i,\sigma} f_{j,\sigma}\rangle$. We obtain a sum of two self-consistent Hamiltonians $H \approx H_{\text{f}} + H_{\text{s}}$:

$$H_{\text{f}} = \sum_{i,j,\sigma} Q_{ij} f^\dagger_{i,\sigma} f_{j,\sigma}, \tag{2a}$$

$$H_{\text{s}} = \sum_{i,j} J_{ij} S^z_i S^z_j + \frac{U}{4} \sum_i S^x_i, \tag{2b}$$

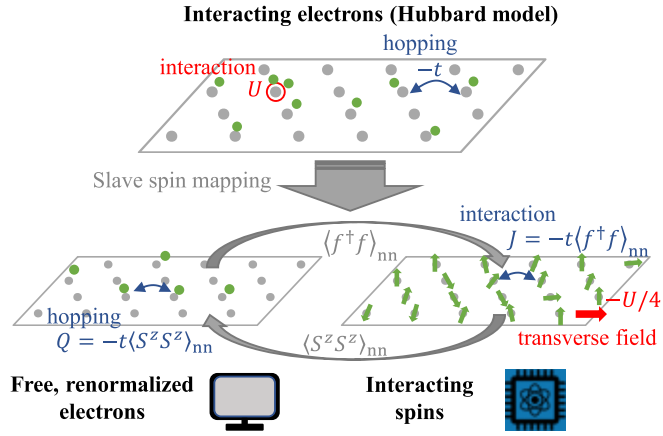

FIG. 1. Slave-spin mapping. The Hubbard Hamiltonian (top) is mapped onto two self-consistently determined simpler problems: an efficiently solvable free-fermionic Hamiltonian with a renormalized hopping [bottom left, $H_{\text{f}}(Q)$ in the text], and a transverse-field Ising Hamiltonian [bottom right, $H_{\text{s}}(J)$ in the text], which we solve using a Rydberg-based quantum processor.

with $Q_{ij} = t_{ij}\langle S^z_i S^z_j\rangle$ and $J_{ij} = \sum_\sigma t_{ij}\langle f^\dagger_{i,\sigma} f_{j,\sigma}\rangle$. In our particle-hole symmetric model, the constraint will be automatically fulfilled at the mean-field level [43,44].

Solving the Hubbard model using slave-spin theory amounts to solving these two self-consistently defined Hamiltonians. This is done iteratively, as illustrated in Fig. 1. We start from an initial guess for the renormalized hopping Q to initiate the self-consistent computation. First, we calculate on a *classical* processor the correlation function $\langle f^\dagger_{i,\sigma} f_{j,\sigma}\rangle$ of the pseudofermion problem, needed to define the spin interaction J_{ij}. The full derivation can be found in the Supplemental Material [45], Sec. II A (see also Refs. [46–50] therein). Second, as the spin problem is hard to solve on a classical processor, we use the analog quantum processor to compute its spin-spin correlation function. Since H_{s} is of infinite size, we first reduce it to a finite-size problem by using a cluster mean-field approximation, as done in, e.g., [51] we solve

$$H^{\mathcal{C}}_{\text{s}} = \sum_{i,j\in\mathcal{C}} J_{ij} S^z_i S^z_j + \frac{U}{4} \sum_{i\in\mathcal{C}} S^x_i + \sum_{i\in\mathcal{C}} h_i S^z_i, \tag{3}$$

where $\mathcal{C}$ denotes the set of N cluster sites and $h_i = 2z_i \overline{J}\,\overline{m}$ is the self-consistent mean field that mimics the influence of the infinite lattice. Here, z_i is the number of neighbors of site i outside the cluster, $\overline{J} = \frac{1}{N_p}\sum_{\langle i,j\rangle\in\mathcal{C}} J_{i,j}$ is the average nearest-neighbor coupling (N_p is the number of nearest-neighbor links inside the cluster), and $\overline{m} = \frac{1}{N}\sum_{i\in\mathcal{C}}\langle S^z_i\rangle$ is the average magnetization. This model needs to be solved iteratively by starting from a guess for the mean field $\overline{m}$. For a given value of this mean field, the finite spin problem defined by $H^{\mathcal{C}}_{\text{s}}$ is solved using a quantum algorithm (described below). This yields the correlation function $\langle S^z_i S^z_j\rangle$ and closes the self-consistent loop, which runs until convergence. At convergence, we extract relevant observables of the original Hubbard model. For instance, the quasiparticle weight Z of the original model, which measures the quantum coherence of the fermionic excitations, is obtained via the spin model's magnetization: $Z = \overline{m}^2$ (we

also have access to site-resolved magnetizations $\langle S_i^z \rangle$ and hence site-resolved quasiparticle weights).

B. Quantum algorithm for the spin Hamiltonian

Let us turn to the solution of the (cluster) spin problem $H_s^{\mathcal{C}}$. It is nothing but the transverse-field Ising model, which could be a candidate problem for reaching quantum advantage using gate-based quantum processors [52]. As it turns out, its form is similar to the Hamiltonian realized experimentally by Rydberg atoms trapped with optical tweezers, for which the geometry of the array can be chosen at will [33]:

$$\hat{H}_{\text{Rydberg}} = \sum_{i \neq j} \frac{C_6}{|\mathbf{r}_i - \mathbf{r}_j|^6} \hat{n}_i \hat{n}_j + \frac{\hbar\Omega(\tau)}{2} \sum_i \hat{S}_i^x - \hbar\delta(\tau) \sum_i \hat{n}_i, \tag{4}$$

where $\Omega(\tau)$ and $\delta(\tau)$ are the time-dependent Rabi frequency and laser detuning, and C_6 the magnitude of the interatomic van der Waals interactions; $\hat{n}_i = (I_i + S_i^z)/2$. Therefore, we can make use of the Rydberg processor to attain the ground state of $H_s^{\mathcal{C}}$ using an annealing procedure:[1] we start from drive parameters $\Omega(\tau = 0) = 0$ and a large positive $\delta(\tau = 0)$ so that the system's native initial state $|\psi_{\text{start}}\rangle = |g\rangle^{\otimes N}$ is the ground state of the initial Hamiltonian. We then, for a long enough annealing time, ramp the Rabi frequency and detuning to reach the final values $\hbar\Omega(\tau_{\max}) = \frac{U}{2}$, $\hbar\delta_i(\tau_{\max}) = \sum_{j \neq i} \frac{C_6}{r_{i,j}^6} - 4\bar{J}\bar{m}z_i$. Optimizing the atom positions in such a way that $\frac{C_6}{r_{i,j}^6} \approx 4J_{i,j}$ (details about this optimization are in the Supplemental Material [45], Sec. III A), the final Hamiltonian will be $H_s^{\mathcal{C}}$. Hence, following the adiabatic theorem, the procedure should (approximately) bring the system to the ground state of $H_s^{\mathcal{C}}$. We can finally measure the spin-spin correlation function on this state.

III. RESULTS

A. Results at equilibrium

We implemented this self-consistent procedure with a realistic numerical simulation of a Rydberg atom processor. We repeated the computation for several values of the local Hubbard interaction U to obtain the evolution of the quasiparticle weight Z as a function of U, as shown in Fig. 2, for cluster sizes, and hence number of atoms, of 4, 6, 8, and 12. Aside from the shot noise, intrinsic to any processor due to the measurement process (the number of measurement is noted N_s), the main experimental limitations were considered in order to account for the true potential of current processors: dephasing noise (with a strength γ), measurement error (characterized by a percentage ϵ), global detuning, finite annealing times

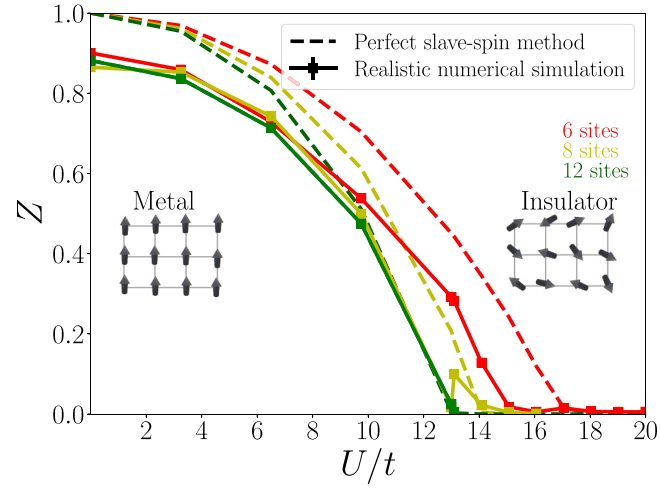

FIG. 2. Mott transition observed with the slave-spin method on a realistic numerical simulation of Rydberg atoms processor. The characteristics of the processor considered are $\tau_{\max} = 4$ μs, $\gamma = 0.02$ MHz, $N_s = 150$, $\epsilon = \epsilon' = 3\%$, and 5×5 loops allowed (see Supplemental Material, Sec. III C [45]). The error bar is the standard error stemming from ϵ and N_s.

$\tau_{\max}$, and imperfect positioning of the atoms to reproduce the right magnetic coupling (see Supplemental Material [45], Sec. III C, for more details). Despite these limitations, leading to few points being far from the noiseless result due to error accumulation, the quasiparticle weight we obtain (solid lines) is in fair agreement with the one obtained from a noiseless solution without shot noise of the spin model (dashed lines). The Rydberg processor can thus be used to get a reasonable estimate of the Mott transition, i.e., the value U_c when Z vanishes and the system turns Mott insulating. While for the half-filled, single-band model studied in this proof-of-concept example, classical methods can be implemented to efficiently solve the spin model (see, e.g., [53]), other regimes are less readily amenable to a controlled classical computation: doped regimes, multiorbital models, and dynamical regimes. We investigate the latter regime in the next paragraph.

B. Results out of equilibrium

We thus turn to a dynamical setting to emphasize the potential advantage brought by the use of quantum processors in this slave-spin framework. Starting from a noninteracting ground state ($U = 0$ MHz), we suddenly switch on the value of the local interaction to a final value U_f. Our goal is to validate that the method implemented on a realistic quantum processor recovers the phenomenology observed in previous experimental and theoretical studies of quenched Hubbard systems [42,43,54–61], such as the collapse and revival oscillations of various observables in the $U_f \gg U_c$ regime, with a $2\pi/U_f$ period, and a damping that increases with bandwidth. In the $U_f \ll U_c$ regime, overdamped oscillations have been observed (see [58] for instance).

Here, we look for this phenomenology in the time evolution of the quasiparticle weight Z. Within the slave-spin method applied to the single-site Hubbard model at half-filling, interaction quenches are simple to implement:

[1]The main difference between $\hat{H}_{\text{Rydberg}}$ and $H_s^{\mathcal{C}}$ is the sign of the interaction: it is positive for Rydberg atoms, negative (since usually $t_{ij} < 0$) for the slave-spin problem. Thus, in practice, parameters are tuned such that the annealing procedure is performed from an initial Hamiltonian of which the system's initial state is its most excited state to the final Hamiltonian $-H_s^{\mathcal{C}}$. The adiabatic theorem can also be applied for the most excited state and therefore the procedure should bring the system to (approximately) the most excited state of $-H_s^{\mathcal{C}}$, i.e., the ground state of $H_s^{\mathcal{C}}$.

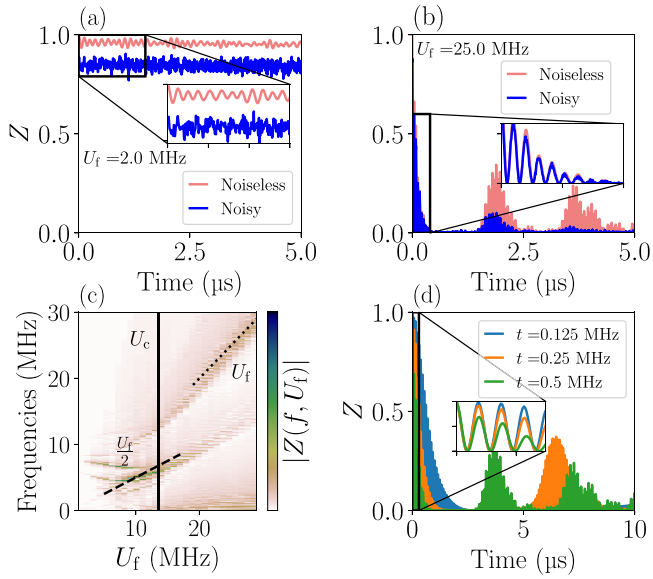

FIG. 3. Dynamical response of the quasiparticle weight after an interaction quench. $N = 12$ spin cluster. Time evolution of Z for (a) $U_f = 2$ MHz and (b) $U_f = 25$ MHz. The red line shows the noiseless annealing solution and the blue line a realistic numerical simulation on Rydberg atoms processor ($\gamma = 0.02$ MHz, $\epsilon = \epsilon' = 3\%$, $N_s = 150$ shots, realistic Ising interactions and a global detuning are imposed). (c) Fourier transform amplitude $|Z(f, U_f)|$. The vertical black line shows the equilibrium critical value U_c as computed from Fig. 2. (d) Impact of the hopping terms t on the damping of the response of Z after a quench ($U_f = 13 \approx U_c$). The blue, orange, and green lines represent the result for $t = 0.125$, 0.25, and 0.5 MHz, respectively.

translation invariance on the lattice makes the dynamics of pseudofermions trivial when starting from an eigenstate (see [42] and the Supplemental Material [45], Sec. I D). Thus, only the dynamics of the spin model are of interest: the procedure boils down to quenching the value of the transverse field in Eq. (3) from 0 to $U_f/4$. On the Rydberg processor considered here, this means switching the Rabi frequency from zero up to the desired value to obtain U_f. In practice, however, the switch-on time is not instantaneous due to the finite temporal response of the optical modulators (about 50 ns to switch from 0 MHz to $U_f = 2$ MHz): we include this effect in our calculations. One then directly measures $\langle S_i^z \rangle$ for different evolution times. In Fig. 3, we show the oscillations observed numerically for a cluster of 12 sites, with and without including the noise. The upper panels present the oscillation of Z as a function of time after a quench to $U_f = 13$ MHz (a) and to $U_f = 25$ MHz (b). From Fig. 2, we know that the phase transition for such a cluster is $U_c \approx 13.5$ MHz. In the case of $U_f = 25$ MHz ($U_f \gg U_c$), we observe the damped oscillations, both in the noiseless and the noisy settings. Because of the dephasing noise present in the experiment and included in the simulation, the agreement between the noiseless and noisy curves worsens with time. However, during the first microseconds of observations, we recover a nearly perfect oscillation from which we can extract the frequency [insets in Figs. 3(a) and 3(b)]. For $U_f = 13$ MHz ($U_f \approx U_c$), we see that Z quickly reaches a value ≈ 0.1 (slightly higher than the Z obtained for this value of U at equilibrium), around which it oscillates. Figure 3(c) exhibits the Fourier transform of $Z(\tau)$ for various U_f for the exact slave-spin method (namely, with an exact solution of the spin model). For $U_f < U_c$, components at $\omega = U_f/2$ can be identified along with other contributions, while for $U_f > U_c$, the component at $\omega = U_f$ dominates the spectrum. This is expected from the physics of the Mott transition in the Hubbard model: above the transition, the single-particle spectrum displays a Mott gap of U_f, while below it excitations between the quasiparticle band and the emerging Hubbard bands (with energy $U_f/2$), and within the quasiparticle band, are possible. Finally, Fig. 3(d) confirms the expected increase of the damping of oscillations with the hopping strength t.

IV. CONCLUSION

In conclusion, we introduced a hybrid quantum-classical method that does not suffer from the usual overheads of translating fermionic problems to spin problems, namely, long quantum evolutions (due to nonlocal spin terms) or auxiliary quantum degrees of freedom. This is made possible by using a slave-spin mapping that turns the difficult fermionic problem into a free, and thus efficiently tractable, fermion problem that is self-consistently coupled to an interacting, yet *local*, spin problem.

Here, to solve the spin problem, we considered an *analog* Rydberg-based quantum processor that naturally implements the effective transverse-field Ising spin Hamiltonian appearing in the slave-spin approach. Its analog character allows one to circumvent the issues associated with gate-based algorithms, like Trotterization when performing time evolution, and the annealing algorithm proposed here avoids the pitfalls of today's widespread variational algorithms like VQE or its temporal counterparts. With the large number of Rydberg atoms that can be controlled in current experiments, this original approach could help tackling problems of (cluster) sizes unreachable to classical computers, without suffering from the limitations that have been pointed out [62–65] in a recent quantum-advantage experimental claim [52]: the atoms can be placed in a two-dimensional array that has high connectivity compared to the quasi-one-dimensional connectivity of the experiments, making tensor network approaches difficult [62], and the correlation lengths that can be attained experimentally in a similar context (up to 7 lattice sites, [28], i.e., 49 spins) also raise the bar for approaches that rely on a smaller effective size [63–65]. This proposal calls for further investigations. An important step would be an experimental validation with larger atom numbers than the 12 atoms we simulated here. Other improvements involve the slave-spin method itself: doped regimes (relevant to cuprate materials), multiorbital models [66] (relevant to iron-based superconductors, where orbital-selective effects may appear [67]) pose various technical difficulties that warrant further theoretical developments. In particular, the fulfillment of the constraint to ensure the states remain in the physical subspace becomes more difficult in these regimes than in the half-filled, single-band case that we studied here. Going beyond the mean-field decoupling of the pseudofermion and spin variables is also another interesting avenue.

ACKNOWLEDGMENTS

We acknowledge fruitful discussions with L.-P. Henry, J. Mikael, M. Schirò, and T. Lahaye. This work has received funding under Horizon Europe programme HORIZON-CL4-2022-QUANTUM-02-SGA via the project 101113690 (PASQuanS2.1), the European Research Council (Advanced Grant No. 101018511-ATARAXIA), and the European High-Performance Computing Joint Undertaking (JU) under Grant Agreement No. 101018180 (HPC-QS). It was also supported by EDF R&D, the Research and Development Division of Electricité de France under the ANRT Contract No. 2020/0011. Simulations were performed on the Eviden Qaptiva platform (ex Atos Quantum Learning Machine).

[1] J. P. F. LeBlanc, A. E. Antipov, F. Becca, I. W. Bulik, G. K.-L. Chan, C.-M. Chung, Y. Deng, M. Ferrero, T. M. Henderson, C. A. Jiménez-Hoyos, E. Kozik, X.-W. Liu, A. J. Millis, N. V. Prokof'ev, M. Qin, G. E. Scuseria, H. Shi, B. V. Svistunov, L. F. Tocchio, I. S. Tupitsyn *et al.*, Solutions of the two-dimensional hubbard model: Benchmarks and results from a wide range of numerical algorithms, Phys. Rev. X **5**, 041041 (2015).

[2] T. Schäfer, N. Wentzell, F. Š. Iv, Y.-Y. He, C. Hille, M. Klett, C. J. Eckhardt, B. Arzhang, V. Harkov, F.-M. LeRegent, A. Kirsch, Y. Wang, A. J. Kim, E. Kozik, E. A. Stepanov, A. Kauch, S. Andergassen, P. Hansmann, D. Rohe, Y. M. Vilk *et al.*, Tracking the footprints of spin fluctuations: A multi-method, multimessenger study of the two-dimensional Hubbard model, Phys. Rev. X **11**, 011058 (2021).

[3] Q. Si, R. Yu, and E. Abrahams, High-temperature superconductivity in iron pnictides and chalcogenides, Nat. Rev. Mater. **1**, 16017 (2016).

[4] E. Y. Andrei, D. K. Efetov, P. Jarillo-Herrero, A. H. MacDonald, K. F. Mak, T. Senthil, E. Tutuc, A. Yazdani, and A. F. Young, The marvels of moiré materials, Nat. Rev. Mater. **6**, 201 (2021).

[5] P. Calabrese and J. Cardy, Evolution of entanglement entropy in one-dimensional systems, J. Stat. Mech. (2005) P04010.

[6] T. Ayral, P. Besserve, D. Lacroix, and E. A. Ruiz Guzman, Quantum computing with and for many-body physics, Eur. Phys. J. A **59**, 227 (2023).

[7] R. P. Feynman, Simulating physics with computers, Int. J. Theor. Phys. **21**, 467 (1982).

[8] U. Schneider, L. Hackermüller, S. Will, T. Best, I. Bloch, T. A. Costi, R. W. Helmes, D. Rasch, and A. Rosch, Metallic and insulating phases of repulsively interacting fermions in a 3D optical lattice, Science **322**, 1520 (2008).

[9] R. Jördens, N. Strohmaier, K. Günter, M. Henning, and T. Esslinger, A Mott insulator of fermionic atoms in an optical lattice, Nature (London) **455**, 204 (2008).

[10] T. Esslinger, Fermi-Hubbard physics with atoms in an optical lattice, Annu. Rev. Condens. Matter Phys. **1**, 129 (2010).

[11] U. Schneider, L. Hackermüller, J. P. Ronzheimer, S. Will, S. Braun, T. Best, I. Bloch, E. Demler, S. Mandt, D. Rasch, and A. Rosch, Fermionic transport and out-of-equilibrium dynamics in a homogeneous Hubbard model with ultracold atoms, Nat. Phys. **8**, 213 (2012).

[12] M. Schreiber, S. S. Hodgman, P. Bordia, H. P. Lüschen, M. H. Fischer, R. Vosk, E. Altman, U. Schneider, and I. Bloch, Observation of many-body localization of interacting fermions in a quasirandom optical lattice, Science **349**, 842 (2015).

[13] R. A. Hart, P. M. Duarte, T.-L. Yang, X. Liu, T. Paiva, E. Khatami, R. T. Scalettar, N. Trivedi, D. A. Huse, and R. G. Hulet, Observation of antiferromagnetic correlations in the Hubbard model with ultracold atoms, Nature (London) **519**, 211 (2015).

[14] L. W. Cheuk, M. A. Nichols, K. R. Lawrence, M. Okan, H. Zhang, E. Khatami, N. Trivedi, T. Paiva, M. Rigol, and M. W. Zwierlein, Observation of spatial charge and spin correlations in the 2D Fermi-Hubbard model, Science **353**, 1260 (2016).

[15] M. Boll, T. A. Hilker, G. Salomon, A. Omran, J. Nespolo, L. Pollet, I. Bloch, and C. Gross, Spin- and density-resolved microscopy of antiferromagnetic correlations in Fermi-Hubbard chains, Science **353**, 1257 (2016).

[16] A. Mazurenko, C. S. Chiu, G. Ji, M. F. Parsons, M. Kanász-Nagy, R. Schmidt, F. Grusdt, E. Demler, D. Greif, and M. Greiner, A cold-atom Fermi–Hubbard antiferromagnet, Nature (London) **545**, 462 (2017).

[17] L. Tarruell and L. Sanchez-Palencia, Quantum simulation of the Hubbard model with ultracold fermions in optical lattices, C. R. Phys. **19**, 365 (2018).

[18] B. Bauer, S. Bravyi, M. Motta, and G. Kin-Lic Chan, Quantum algorithms for quantum chemistry and quantum materials science, Chem. Rev. **120**, 12685 (2020).

[19] Y. Cao, J. Romero, J. P. Olson, M. Degroote, P. D. Johnson, M. Kieferová, I. D. Kivlichan, T. Menke, B. Peropadre, N. P. D. Sawaya, S. Sim, L. Veis, and A. Aspuru-Guzik, Quantum chemistry in the age of quantum computing, Chem. Rev. **119**, 10856 (2019).

[20] P. Jordan and E. Wigner, Íber das Paulische äquivalenzverbot, Z. Phys. **47**, 631 (1928).

[21] S. B. Bravyi and A. Y. Kitaev, Fermionic quantum computation, Ann. Phys. **298**, 210 (2002).

[22] F. Verstraete and J. I. Cirac, Mapping local Hamiltonians of fermions to local Hamiltonians of spins, J. Stat. Mech. (2005) P09012.

[23] K. Setia, S. Bravyi, A. Mezzacapo, and J. D. Whitfield, Superfast encodings for fermionic quantum simulation, Phys. Rev. Res. **1**, 033033 (2019).

[24] C. Derby, J. Klassen, J. Bausch, and T. Cubitt, A compact fermion to qubit mapping, Phys. Rev. B **104**, 035118 (2021).

[25] K. Bharti, A. Cervera-Lierta, T. H. Kyaw, T. Haug, S. Alperin-Lea, A. Anand, M. Degroote, H. Heimonen, J. S. Kottmann, T. Menke, W.-K. Mok, S. Sim, L.-C. Kwek, and A. Aspuru-Guzik, Noisy intermediate-scale quantum algorithms, Rev. Mod. Phys. **94**, 015004 (2022).

[26] S. Endo, Z. Cai, S. C. Benjamin, and X. Yuan, Hybrid quantum-classical algorithms and quantum error mitigation, J. Phys. Soc. Jpn. **90**, 032001 (2021).

[27] A. Peruzzo, J. McClean, P. Shadbolt, M.-H. Yung, X.-Q. Zhou, P. J. Love, A. Aspuru-Guzik, and J. L. O'Brien, A variational eigenvalue solver on a quantum processor, Nat. Commun. **5**, 4213 (2013).

[28] P. Scholl, M. Schuler, H. J. Williams, A. A. Eberharter, D. Barredo, K.-N. Schymik, V. Lienhard, L.-P. Henry, T. C. Lang, T. Lahaye, A. M. Läuchli, and A. Browaeys, Quantum simulation of 2D antiferromagnets with hundreds of Rydberg atoms, Nature (London) **595**, 233 (2021).

[29] C. Chen, G. Bornet, M. Bintz, G. Emperauger, L. Leclerc, V. S. Liu, P. Scholl, D. Barredo, J. Hauschild, S. Chatterjee, M. Schuler, A. M. Läuchli, M. P. Zaletel, T. Lahaye, N. Y. Yao, and A. Browaeys, Continuous symmetry breaking in a two-dimensional Rydberg array, Nature (London) **616**, 691 (2023).

[30] S. Ebadi, T. T. Wang, H. Levine, A. Keesling, G. Semeghini, A. Omran, D. Bluvstein, R. Samajdar, H. Pichler, W. W. Ho, S. Choi, S. Sachdev, M. Greiner, V. Vuletić, and M. D. Lukin, Quantum phases of matter on a 256-atom programmable quantum simulator, Nature (London) **595**, 227 (2021).

[31] A. W. Glaetzle, M. Dalmonte, R. Nath, C. Gross, I. Bloch, and P. Zoller, Designing frustrated quantum magnets with laser-dressed rydberg atoms, Phys. Rev. Lett. **114**, 173002 (2015).

[32] D. Bluvstein, A. Omran, H. Levine, A. Keesling, G. Semeghini, S. Ebadi, T. T. Wang, A. A. Michailidis, N. Maskara, W. W. Ho, S. Choi, M. Serbyn, M. Greiner, V. Vuletić, and M. D. Lukin, Controlling quantum many-body dynamics in driven Rydberg atom arrays, Science **371**, 1355 (2021).

[33] A. Browaeys and T. Lahaye, Many-body physics with individually controlled Rydberg atoms, Nat. Phys. **16**, 132 (2020).

[34] I. Bloch, J. Dalibard, and W. Zwerger, Many-body physics with ultracold gases, Rev. Mod. Phys. **80**, 885 (2008).

[35] D. González-Cuadra, D. Bluvstein, M. Kalinowski, R. Kaubruegger, N. Maskara, P. Naldesi, T. V. Zache, A. M. Kaufman, M. D. Lukin, H. Pichler, B. Vermersch, J. Ye, and P. Zoller, Fermionic quantum processing with programmable neutral atom arrays, Proc. Natl. Acad. Sci. USA **120**, e2304294120 (2023).

[36] C. Kokail, C. Maier, R. van Bijnen, T. Brydges, M. K. Joshi, P. Jurcevic, C. A. Muschik, P. Silvi, R. Blatt, C. F. Roos, and P. Zoller, Self-verifying variational quantum simulation of the lattice Schwinger model, Nature (London) **569**, 355 (2019).

[37] J. Argüello-Luengo, A. González-Tudela, T. Shi, P. Zoller, and J. I. Cirac, Analogue quantum chemistry simulation, Nature (London) **574**, 215 (2019).

[38] A. Michel, S. Grijalva, L. Henriet, C. Domain, and A. Browaeys, Blueprint for a digital-analog variational quantum eigensolver using Rydberg atom arrays, Phys. Rev. A **107**, 042602 (2023).

[39] L. Henriet, L. Beguin, A. Signoles, T. Lahaye, A. Browaeys, G.-O. Reymond, and C. Jurczak, Quantum computing with neutral atoms, Quantum **4**, 327 (2020).

[40] D. Wu, R. Rossi, F. Vicentini, N. Astrakhantsev, F. Becca, X. Cao, J. Carrasquilla, F. Ferrari, A. Georges, M. Hibat-Allah, M. Imada, A. M. Läuchli, G. Mazzola, A. Mezzacapo, A. Millis, J. R. Moreno, T. Neupert, Y. Nomura, J. Nys, O. Parcollet *et al.*, Variational benchmarks for quantum many-body problems, arXiv:2302.04919.

[41] A. Rüegg, S. D. Huber, and M. Sigrist, Z_2-slave-spin theory for strongly correlated fermions, Phys. Rev. B **81**, 155118 (2010).

[42] M. Schiró and M. Fabrizio, Quantum quenches in the Hubbard model: Time-dependent mean-field theory and the role of quantum fluctuations, Phys. Rev. B **83**, 165105 (2011).

[43] W.-W. Yang, H.-G. Luo, and Y. Zhong, Benchmarking the simplest slave-particle theory with Hubbard dimer, Chin. Phys. B **28**, 107103 (2019).

[44] L. de' Medici and M. Capone, Modeling many-body physics with slave-spin mean-field: Mott and hund's physics in fe-superconductors, in *The Iron Pnictide Superconductors: An Introduction and Overview*, edited by F. Mancini and R. Citro (Springer, Berlin, 2017), pp. 115–185.

[45] See Supplemental Material at http://link.aps.org/supplemental/10.1103/PhysRevB.109.174409 for details on the implementation of the slave-spin method on a realisitic RQP; studies of the impact of each source of noise considered on the result and theoretical considerations to prove the viability of the implementation.

[46] P. Virtanen, R. Gommers, T. E. Oliphant, M. Haberland, T. Reddy, D. Cournapeau, E. Burovski, P. Peterson, W. Weckesser, J. Bright, S. J. van der Walt, M. Brett, J. Wilson, K. J. Millman, N. Mayorov, A. R. J. Nelson, E. Jones, R. Kern, E. Larson, C. J. Carey *et al.*, SciPy 1.0: Fundamental algorithms for scientific computing in python, Nat. Methods **17**, 261 (2020).

[47] J. R. Johansson, P. D. Nation, and F. Nori, QuTiP 2: A Python framework for the dynamics of open quantum systems, Comput. Phys. Commun. **184**, 1234 (2013).

[48] S. de Léséleuc, D. Barredo, V. Lienhard, A. Browaeys, and T. Lahaye, Analysis of imperfections in the coherent optical excitation of single atoms to Rydberg states, Phys. Rev. A **97**, 053803 (2018).

[49] V. Lienhard, S. de Léséleuc, D. Barredo, T. Lahaye, A. Browaeys, M. Schuler, L.-P. Henry, and A. M. Läuchli, Observing the space- and time-dependent growth of correlations in dynamically tuned synthetic Ising models with antiferromagnetic interactions, Phys. Rev. X **8**, 021070 (2018).

[50] H. Silvério, S. Grijalva, C. Dalyac, L. Leclerc, P. J. Karalekas, N. Shammah, M. Beji, L.-P. Henry, and L. Henriet, Pulser: An open-source package for the design of pulse sequences in programmable neutral-atom arrays, Quantum **6**, 629 (2022).

[51] S. R. Hassan and L. de' Medici, Slave spins away from half filling: Cluster mean-field theory of the Hubbard and extended Hubbard models, Phys. Rev. B **81**, 035106 (2010).

[52] Y. Kim, A. Eddins, S. Anand, K. X. Wei, E. van den Berg, S. Rosenblatt, H. Nayfeh, Y. Wu, M. Zaletel, K. Temme, and A. Kandala, Evidence for the utility of quantum computing before fault tolerance, Nature (London) **618**, 500 (2023).

[53] M. Schuler, S. Whitsitt, L.-P. Henry, S. Sachdev, and A. M. Läuchli, Universal signatures of quantum critical points from finite-size torus spectra: A window into the operator content of higher-dimensional conformal field theories, Phys. Rev. Lett. **117**, 210401 (2016).

[54] M. Greiner, O. Mandel, T. W. Hänsch, and I. Bloch, Collapse and revival of the matter wave field of a Bose–Einstein condensate, Nature (London) **419**, 51 (2002).

[55] C. Kollath, A. M. Läuchli, and E. Altman, Quench dynamics and nonequilibrium phase diagram of the Bose-Hubbard model, Phys. Rev. Lett. **98**, 180601 (2007).

[56] J. Schachenmayer, A. J. Daley, and P. Zoller, Atomic matter-wave revivals with definite atom number in an optical lattice, Phys. Rev. A **83**, 043614 (2011).

[57] M. Lacki and M. Heyl, Dynamical quantum phase transitions in collapse and revival oscillations of a quenched superfluid, Phys. Rev. B **99**, 121107(R) (2019).

[58] M. Eckstein, M. Kollar, and P. Werner, Thermalization after an interaction quench in the Hubbard model, Phys. Rev. Lett. **103**, 056403 (2009).

[59] D. Iyer, R. Mondaini, S. Will, and M. Rigol, Coherent quench dynamics in the one-dimensional Fermi-Hubbard model, Phys. Rev. A **90**, 031602(R) (2014).

[60] S. Will, D. Iyer, and M. Rigol, Observation of coherent quench dynamics in a metallic many-body state of fermionic atoms, Nat. Commun. **6**, 6009 (2015).

[61] L. Riegger, G. Orso, and F. Heidrich-Meisner, Interaction quantum quenches in the one-dimensional Fermi-Hubbard model with spin imbalance, Phys. Rev. A **91**, 043623 (2015).

[62] J. Tindall, M. Fishman, E. M. Stoudenmire, and D. Sels, Efficient tensor network simulation of IBM's eagle kicked Ising experiment, PRX Quantum **5**, 010308 (2024).

[63] T. Begušić, J. Gray, and G. K.-L. Chan, Fast and converged classical simulations of evidence for the utility of quantum computing before fault tolerance, Sci. Adv. **10**, eadk4321 (2024).

[64] K. Kechedzhi, S. Isakov, S. Mandrà, B. Villalonga, X. Mi, S. Boixo, and V. Smelyanskiy, Effective quantum volume, fidelity and computational cost of noisy quantum processing experiments, Future Generation Computer Systems **153**, 431 (2024).

[65] E. G. D. Torre and M. M. Roses, Dissipative mean-field theory of IBM utility experiment, arXiv:2308.01339.

[66] L. de'Medici, A. Georges, and S. Biermann, Orbital-selective Mott transition in multiband systems: Slave-spin representation and dynamical mean-field theory, Phys. Rev. B **72**, 205124 (2005).

[67] L. de' Medici, G. Giovannetti, and M. Capone, Selective mott physics as a key to iron superconductors, Phys. Rev. Lett. **112**, 177001 (2014).